

# Classifying High-Energy Celestial Objects with Machine Learning Methods

Nolan Faught

Tyrian Hobbs

Alexis Mathis

Daniel Yu

Department of Mathematics, Northeastern University

December 15, 2025

## Abstract

Machine learning is a field that has been growing in importance since the early 2010s due to the increasing accuracy of classification models and hardware advances that have enabled faster training on large datasets. In the field of astronomy, tree-based models and simple neural networks have recently garnered attention as a means of classifying celestial objects based on photometric data. We apply common tree-based models to assess performance of these models for discriminating objects with similar photometric signals, pulsars and black holes.

We also train a RNN on a downsampled and normalized version of the raw signal data to examine its potential as a model capable of object discrimination and classification in real-time.

## 1 Introduction

Modern astronomy has generated an extensive taxonomy of celestial objects based on their physical characteristics and predicted future state. As theories of the development, expansion, history, and predicted future state of the universe rely on identifying and observing celestial bodies, it is essential to have quick and accurate classification of newly observed objects. Historically, classification was performed manually, but the rapid expansion of modern catalogues of celestial objects – such as the Sloan Digital Sky Survey, which grows at a rate of thousands of entries daily [1] – makes this manual classification impractical.

Supervised and semi-supervised machine learning represent the most promising candidates for the desired computational classification. Until recently, the data, hardware, and software required for large-scale training and deployment of these methods were unavailable to the general research community. However, improvements to parallel processing hardware have driven increased success and adoption, resulting in the invention of models capable of equaling or surpassing human-level intelligence in tasks formerly considered intractable to computers. Such improvements have been recognized in facial recognition [2] and combinatorial game theory [3], but despite their meteoric rise in popularity, there is a significant gap in astronomical literature on applying machine learning models to the problem of celestial object classification.

In an effort to improve this state, we explore a number of machine learning based models for a simplified celestial object classification problem to assess the performance and potential of these models in the field of astronomy.

## 2 Literature Review

Previous work has applied convolutional neural networks [4] and tree-based models to classification problems in broader categories [5] using photometric data. Models that rely on features extracted from photometric data, such as gravitational tensors, have also gained attention [6], [7]. However, there seems to be a gap in the literature in applying tree-based models to discriminate more photometrically similar object classes, such as black holes and pulsars.

This work attempts to address this gap by examining both previously considered computational discrimination models in a more specific task environment to address their performance, and additionally explores a recurrent neural network model trained directly on downsampled photometric digital signals with the intention of creating a model capable of real-time inference.

### 3 Background

Celestial objects are classified by the characteristics of their emitted and reflected light. By examining the spectra and patterns of the light curve – the time-varying signal of frequency and intensity from a single object – it is possible to determine the mass, momentum, rotation, gravitational field, and composition of an object with high accuracy and precision. Modern high-powered telescopes record digital signals in both high- and low-frequency bands of the electromagnetic spectrum, providing viable data to characterize these objects.

Two particular celestial objects are difficult to discriminate due to their similar photometric signals: black holes and pulsars. A black hole is a celestial object so dense that nothing – even light – can escape from its gravitational pull. What we view is the accretion disk, a layer of rapidly-spinning material that is heated by friction and shines brightly. A pulsar is a rotating neutron star that emits jets of matter and electromagnetic radiation from its magnetic poles. Much like a lighthouse, the rotation of the neutron stars periodically sweeps these cones of light in the direction of the Earth, causing us to see a pulsating star, or a pulsar. These pulses occur at very regular intervals, typically ranging from milliseconds to seconds.

Theoretically, the electromagnetic signal received from a black hole is constant, with occasional spikes due to jets of escaped material. Pulsars, on the other hand, should exhibit a sinusoidal light curve with regular spikes corresponding to the times the pulsar's magnetic poles are facing the earth. In practice, owing to cosmic noise and other visual factors, these two objects can be difficult to distinguish without careful consideration.

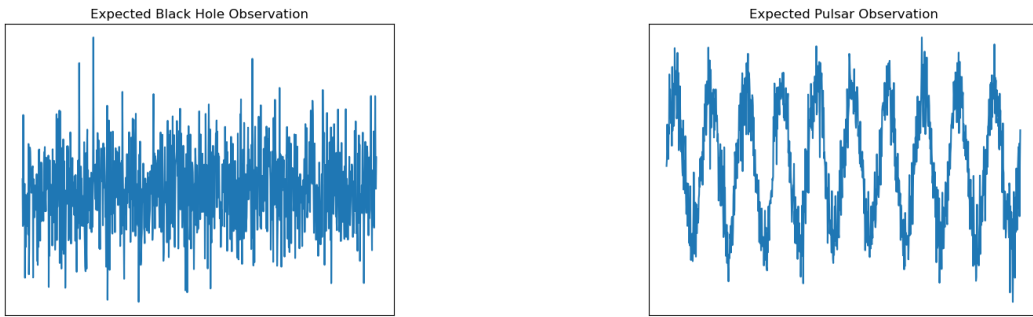


Figure 1: Ideal Light Curves

Our models are trained on the photometric signals of black holes and pulsars in the hard X-ray band, a high-frequency band of the EM spectrum. These data are all provided from the same instrument, the Nuclear Spectroscopic Telescope Array (NuSTAR), a NASA telescope which has been performing observational research on a variety of objects in the X-ray wavelength since 2012. [8] It has greater sensitivity compared to previous instruments operating in similar energy bands, making it particularly useful for study of celestial objects.

### 4 Methodology

Target sources for this study included supermassive black holes and millisecond pulsars selected based on their observational characteristics and scientific interest. Data were acquired via the High Energy Astrophysics Science Archive Research Center (HEASARC) browsing system by querying the NuSTAR mission master database for all publicly available observations of the selected targets; the full list of objects viewed and their number of suitable observations is listed in the appendix. For each observation meeting selection criteria, cleaned event files were retrieved from the archive.

The event format (.evt) is a file format common to astronomical data used to store a telescope's recorded output. Necessary for this analysis was the pixel location, UTC time, and pulse-invariant (PI) channel of incoming events (photons). NuSTAR provides event files that have been processed to remove sources of measurement error such as cross-correlation between pixels and shifts to the spectra caused by exposure variations, as documented in the NuSTAR software guide [9].

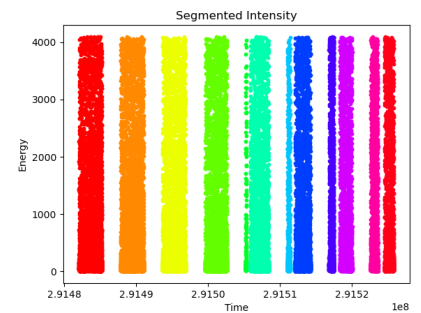
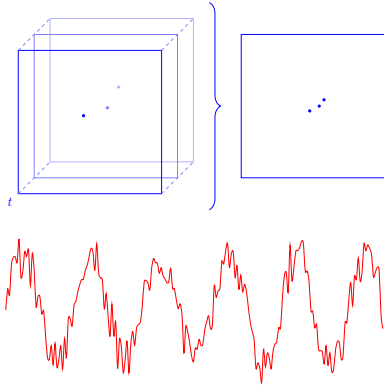


Figure 2: Gaps in event arrival times (colored by cluster)

NuSTAR's cleaning process also includes removal of "dirty" data; this may occur due to instrument dead time, telescope movement, the satellite passing through high-radiation sections of space (such as the South Atlantic Anomaly), or any other event that may damage data quality. Thus, our observations contained large gaps between portions of usable data, often around three thousand seconds in length.

Otherwise, events occurred at 0.25s to 0.65s intervals, with a median wait time of 0.5s. A histogram analysis revealed that arrival times appeared to follow a Poisson distribution with an approximate rate of 0.5s.

## 4.1 Preprocessing and Normalization



*Top:* Integration of sparse signal matrices over time

*Bottom:* Real-valued signal at a constant period

The digital signals were reconstructed as dense  $k \times n \times n$  real-valued tensors, where  $k$  represented event time and  $n \times n$  represented the spatial aperture (camera pixels), zero-padded to a uniform size. An initial reconstruction approach consisted of integrating photon arrivals at constant periods with  $T \in \{0.5, 1, 5, 15, 30\}$  second intervals, but the resulting signals proved too sparse to perform analysis. Spatial downsampling, filtering, and smoothing methods were considered as potential alternatives, but ultimately rejected as outside the scope of this work.

Since there is no expected difference in shape between the two celestial objects, the spatial characteristics of photon arrivals were ultimately discarded. Instead, the energy of the events were integrated over time to create a real-valued signal with a constant period of one second. This period was selected after experimentation as the shortest interval capable of producing signals with sufficient density for analysis. The resulting signals were first segmented at the aforementioned data gaps, then processed with a sliding-window approach with thirty minute (1800s) windows and a thirty second stride.

For feature-based models, analysis of the  $k$  largest Fourier coefficients was considered, but again proved outside the scope of this research. Instead, ten statistical features were extracted from each processed intensity signal. These consisted of sample mean, the five quartile values, standard deviation, variation, skewness, and kurtosis.

## 4.2 Data Exploration

The finalized intensity dataset consisted of 1800 features, one for each second of the thirty-minute (1800s) observation interval, and the target label (pulsar or black hole). There was an approximate 3:1 class imbalance, with black hole observations significantly outnumbering pulsars.

The figure below shows sample time series of a randomly selected black hole and pulsar. Compared to the ideal theoretical distributions, the observed sample distributions are notably difficult to distinguish; there are no significant differences in amplitude distribution, cycle length, or baseline drift that could potentially allow for class separation through visual inspection or linear separation. This similarity demonstrates the utility of machine intervention.

Examining the summary statistics described above, second-order summaries were computed across their distribution, and compared between the two classes. The difference between the averages for each feature is visible on the right, alongside the logarithmic scale.

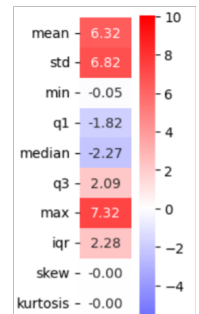


Figure 3:  
Average Statistic Differences

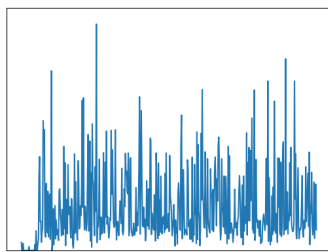


Figure 4: Sample Black Hole

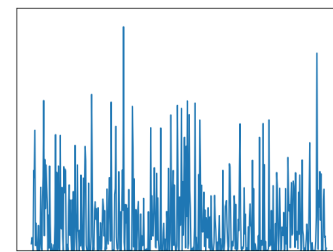


Figure 5: Sample Pulsar

Pulsars demonstrated on average far higher means, standard deviations, and max values, and had lower first quartiles and medians. Skewness and kurtosis showed no major differences; this is unsurprising, as both were on a very small scale, and the intensity curves were generally cyclic.

These findings indicate that pulsars produce infrequent but strong high-amplitude pulses, while their median behavior remains more muted.

### 4.3 Models

Following from the general tendencies present in previous literature, three models were trained based on the statistical features: a logistic regression model, a random forest model, and XGBoost. These models were trained with cloud computing resources provided by the collaborative scientific research platform SciServer.

Finally, a recurrent neural network was trained directly on the downsampled signal data. While convolutional and deep neural networks were considered, the time-dependent nature of the data demonstrated a clear suitability for recurrent neural networks. Due to computational limitations of SciServer, this model was trained on physical hardware, as discussed further below.

Since the dataset contained a class imbalance favoring black holes over pulsars, training and validation data was stratified to help account for this disparity.

#### 4.3.1 Logistic Regression

Logistic regression models the log-odds of the class probability as a linear combination of the input features. Because the model is inherently linear, it cannot capture nonlinear patterns or feature interactions unless nonlinear or interaction features are explicitly constructed and provided as inputs.

The logistic regression was trained for 1000 iterations.

#### 4.3.2 Random Forest

The second model trained was a random forest, created using the summary statistics dataset and the scikit-learn RandomForestClassifier module.

RandomForestClassifier trains decision trees based on random subsets of the available features, then aggregates their outputs to create a final decision. Our training created one hundred such decision trees, utilizing three randomly chosen features to make each splitting decision. Decisions were made based on improving the Gini purity of bootstrapped samples the same size as the initial dataset. We did not set a max tree depth, instead allowing the decision tree to continue splitting until the nodes were completely pure.

#### 4.3.3 XGBoost

The third model trained was an XGBoost (eXtreme Gradient Boosting) classifier, which builds an ensemble of decision trees sequentially. Each new tree is trained on the gradient (and second-order gradient) of the loss with respect to the current model's predictions, allowing it to correct the residual errors made by the previous trees.

For our model, we decided to use a standard learning rate of 0.05 and a sequence of 400 trees with each tree at a maximum depth of 10 branches. In order to minimize overfitting, we randomly sample only 80 percent of the data and 80 percent of the features for each tree created in the ensemble. Similarly, we also re-weight the imbalanced classes.

This combination of parameters were chosen to prevent overfitting while maximizing accuracy.

#### 4.3.4 RNN

Our most complicated model was a bidirectional Long Short-Term Memory (LSTM) recurrent neural network (RNN) trained on photometric signals normalized with z-score scaling.

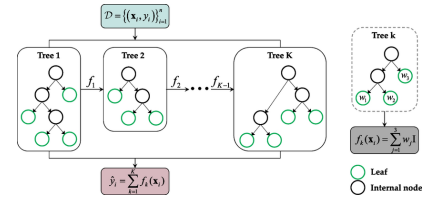


Figure 6: XGBoost Architecture

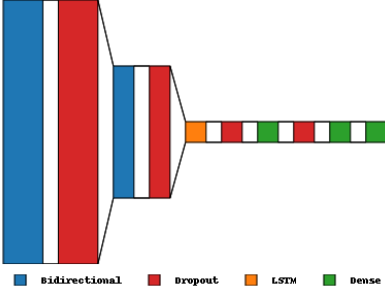


Figure 7: RNN Architecture

The structure of the RNN contains ten layers: 2 bidirectional LSTM, 1 standard LSTM, 3 dense, and 4 dropouts. Multiple LSTM layers were used to increase the opportunity that the RNN would extract the important features of the signal as simpler signals. Bidirectional LSTM layers were included due to their effectiveness at distinguishing features of periodic signals. Dropout layers turned off 30% neurons three times and 40% of neurons once during the third iteration of training. Two of the dense layers used a ReLU activation function, and the final layer a sigmoid activation.

The model was trained using the Adam optimizer with binary cross-entropy loss. Training, test, and validation performance were assessed with model accuracy. Due to the volume of data and temporal requirements for training the model, this model was trained on a physical desktop with a 12-core CPU and 64GiB RAM. Training took about 11 continuous hours of operation at 1.2 CPU core usage, requiring 24GiB of memory.

The RNN model was trained twice on subsets of the data. The first training period was performed on 5 objects and took about 2 hours to complete. The results of this training period were trained on 60% of the remaining data.

## 5 Results

### 5.1 Logistic Regression

Logistic regression was adopted as the baseline model and attained a training accuracy of 0.711 and a test accuracy of 0.71, indicating the model has generalized well from training to test data. However, the confusion matrix shows that the model is misclassifying a significant number of black holes as pulsars. This tradeoff for increased sensitivity to the minority class, pulsars (1), at the cost of reduced accuracy for the majority class, black holes (0), is explained by the re-weighting of the model to correct for the class imbalance.

The model's inability to simultaneously improve accuracy on both classes suggests that the underlying decision boundary is not well-approximated by a linear separator. In such settings, logistic regression exhibits high model bias and cannot capture the complex, nonlinear structure present in the data. Thus models such as Random Forest or XGBoost should result in improved performance.

### 5.2 Random Forest

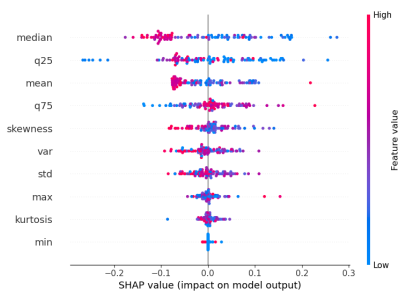


Figure 9: Random Forest SHAP values

The random forest model achieved an initial training accuracy of 1, which is not uncommon for random forest models in general. The random forest model achieved a total test accuracy of 0.931. It had precision of 0.94 and recall of 0.97 with black holes, and precision of 0.90 and recall of 0.84 with pulsars. It assigned highest importance to the median with a feature importance value of 0.1873, followed by the 25th quartile and the mean with feature importances 0.1523 and 0.13 respectively.

Unfortunately, this also came with an average tree depth of 42.7 splits (minimum 38, maximum 53). These large trees increase computational time, reduce interpretability, and while the random nature of the training helps combat overfitting it is still a potential problem. Nevertheless, this is a promising result that suggests more exploration.

### 5.3 XGBoost

XGBoost achieved 0.938 accuracy on the training set and 0.92 accuracy on the test set, similar in accuracy to the random forest model. Trees were shallower compared to the random forest, which we conjecture has resulted in less overfitting.

Examining the confusion matrix, the model had a slight tendency to misclassify black holes towards pulsars. However, this is not significant and accuracy in both pulsar and black hole classification improved compared to the logistic regression model, indicating the model picked up on nonlinear interactions that logistic regression was unable to.

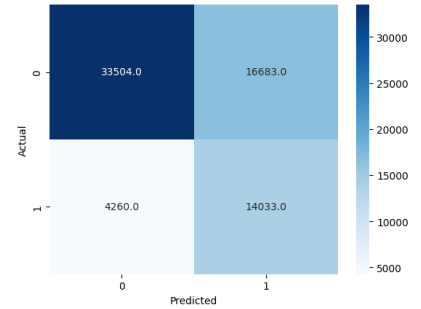


Figure 8: Logistic Regression Confusion Matrix

The SHAP values coincide with the values for the Random Forest model. The top two features are identical and three out of five top features are the same. The features picked out as important all describe the central tendency and tail behavior of the distribution, which is consistent with the analysis during data exploration. Specifically, the models agree that pulsars tend to have higher medians, sharper peaks, and greater variance. However, while the models pick up similar non linear patterns, XGBoost seems to have more outliers in terms of model impact than the random forest.

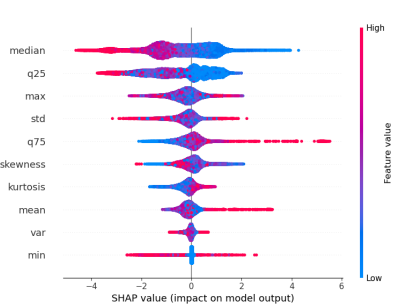


Figure 10: XGBoost SHAP Values

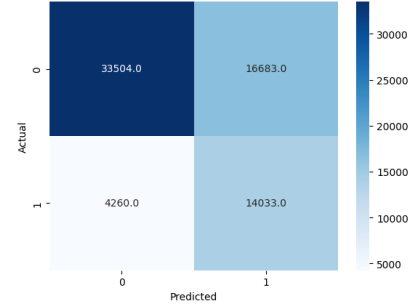


Figure 11: XGBoost Confusion Matrix

## 5.4 Recurrent Neural Network

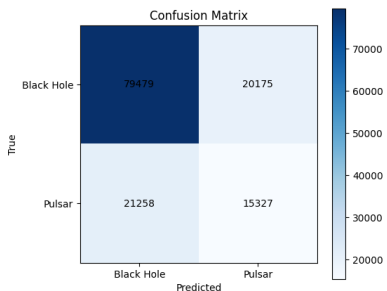


Figure 12: RNN confusion matrix for large dataset

The recurrent neural network demonstrated high training accuracy at 0.91 but low test accuracy at 0.69. This is likely an artifact of overfitting, but due to time constraints we were unable to retrain the model or attempt to refine the training process. Adjustments to the structure or data pre-processing that may improve results are discussed in section 6.1.

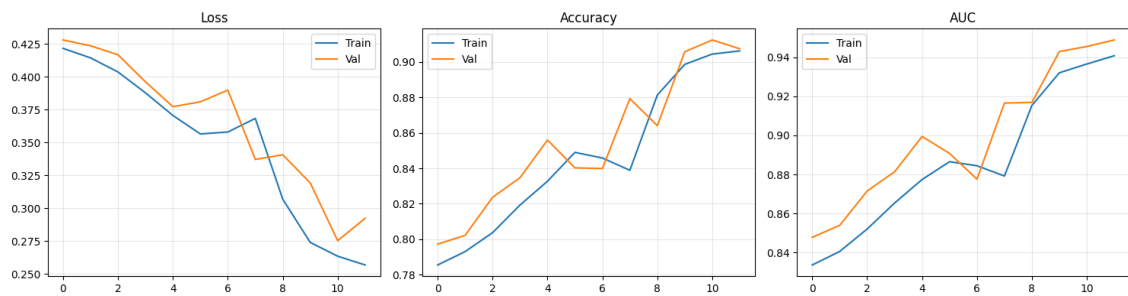


Figure 13: Loss, accuracy, and AUC of the training and validation

## 5.5 Model Cross-Comparison

Model	Training Accuracy	Test Accuracy	Training Time
Logistic Regression	0.711	0.71	4m 24.62s
Random Forest	1.00	0.931	1m 6.12s
XGBoost	0.938	0.92	1m 1.18s
RNN	0.91	0.69	10hr 49m

## 6 Discussion

Tree-based models had comparable accuracy and precision to other models in the literature, which shows that tree-based models are apt for more specific celestial object discrimination. The simplicity of our data pre-processing and lack of signal processing are a weakness of our approach, so more accurate and mathematically rigorous models should demonstrate improved performance.

The accuracy of the recurrent neural network showed steady improvement prior to stopping the training period. Tuning the downsampling or combining spatial aspects of the signal to produce a combined recurrent-convolutional neural network may be viable approaches for real-time signal processing, but the current results are inconclusive.

Our results show that a purely ML approach to classifying pulsars and black holes is indeed viable and can classify pulsars and black holes to a high degree of accuracy.

### 6.1 Further Work

The use of statistical methods for digital signals may be a significant source of error due to cross-correlation of features in time. The mean and median, in particular, are unreliable for discrimination problems due to correlating directly to distance from the Earth.

Examining the tuning, training, and structure of the recurrent neural network proved too computationally intensive for in-depth analysis. Improvements that we considered include mostly the pre-processing and cleaning of signals, such as spatial filtering, clutter removal, spatial/temporal smoothing, and larger intervals between signal sampling.

## 7 Acknowledgments

This research has made use of data, software and/or web tools obtained from the High Energy Astrophysics Science Archive Research Center (HEASARC), a service of the Astrophysics Science Division at NASA/GSFC and of the Smithsonian Astrophysical Observatory's High Energy Astrophysics Division.

This research made use of the SciServer science platform ([www.sciserver.org](http://www.sciserver.org)). SciServer is a collaborative research environment for large-scale data-driven science. It is being developed at, and administered by, the Institute for Data Intensive Engineering and Science at Johns Hopkins University. SciServer is funded by the National Science Foundation through the Data Infrastructure Building Blocks (DIBBs) program and others, as well as by the Alfred P. Sloan Foundation and the Gordon and Betty Moore Foundation.

This research has used programming assistance provided by Anthropic's Claude Sonnet 4.5 model. All outputs were confirmed by a researcher and no AI assistance was used for interpretation, review, or final reporting.

This research was largely possible due to the open-source programming library Scikit-learn. We would like to thank the creators and maintainers of that module for support of the academic community.

## References

- [1] D. G. York et al., "The Sloan Digital Sky Survey: Technical summary," *The Astronomical Journal*, vol. 120, no. 3, p. 1579, 2000.
- [2] O. Parkhi, A. Vedaldi, and A. Zisserman, "Deep face recognition," in *BMVC 2015-Proceedings of the British Machine Vision Conference 2015*, British Machine Vision Association, 2015.

- [3] F.-h. Hsu, M. S. Campbell, and A. J. Hoane Jr, “Deep blue system overview,” in *Proceedings of the 9th international conference on Supercomputing*, 1995, pp. 240–244.
- [4] H. Gaikwad, N. Mhala, A. Umare, A. Milimile, and A. Lanjewar, “Classification of star and galaxy objects utilizing machine learning techniques and deep neural networks,” in *Advances in Distributed Computing and Machine Learning*, U. Nanda, A. K. Tripathy, J. P. Sahoo, M. Sarkar, and K.-C. Li, Eds., Singapore: Springer Nature Singapore, 2024, pp. 13–23, ISBN: 978-981-97-3523-5.
- [5] F. Z. Zeraatgari et al., *Machine learning-based photometric classification of galaxies, quasars, emission-line galaxies, and stars*, 2023. arXiv: 2311.02951 [astro-ph.GA]. [Online]. Available: <https://arxiv.org/abs/2311.02951>
- [6] M. F. Siddiquee and M. M. Hasan, “Spectral and morphological classification of celestial objects using physics informed machine learning,” in *2024 IEEE 3rd International Conference on Robotics, Automation, Artificial-Intelligence and Internet-of-Things (RAAICON)*, 2024, pp. 7–12. DOI: 10.1109/RAAICON64172.2024.10928692
- [7] S. P. Omprakash Barapatre Shubham Sanskar Routray, “A physics-informed hybrid machine learning pipeline for celestial object classification,” *IJRTI*, 2025.
- [8] NuSTAR Science Operations Center, *NuSTAR – Nuclear Spectroscopic Telescope Array*, <https://nustar.caltech.edu/>, Accessed: 2025-12-09, 2025.
- [9] M. Perri et al., “The nustar data analysis software guide,” *ASI Space Science Data Center and California Institute of Technology (Julio 2021)*, 2013.
- [10] N. White and S. S. Murray, “Heasarc software archive,” 2003.
- [11] A. T. Hassina, “Using machine learning to classify and localize stellar objects,” *viXra*, Aug. 2023.
- [12] F. Pedregosa et al., “Scikit-learn: Machine learning in Python,” *Journal of Machine Learning Research*, vol. 12, pp. 2825–2830, 2011.

## 8 Appendix

Object Name	Object Type	Number of Observations
3C 264	Black Hole	2
APM 08279	Black Hole	4
Centaurus A*	Black Hole	12
M87*	Black Hole	38
MCG-6-30-15	Black Hole	12
NGC 1275	Black Hole	4
NGC 4151	Black Hole	26
NGC 4388	Black Hole	2
NGC 4579	Black Hole	2
Sag A*	Black Hole	152
IC10	Pulsar	6
IGR J00291	Pulsar	2
M82 X2	Pulsar	16
NGC 2808, MAXI J0911	Pulsar	6
NGC 5907	Pulsar	30
NGC 6397	Pulsar	2
NGC 6440, IGR J 17488	Pulsar	2
NGC 6441, 4U 1746	Pulsar	2
NGC 6626, PSR B1821	Pulsar	10
PSR B0833	Pulsar	2
Terzan 5	Pulsar	2

Table 1: Celestial Objects acquired from HEASARC